Contrib Mineral Petrol (2006) 152:667–684
DOI 10.1007/s00410-006-0126-z

ORIGINAL PAPER

Fractionation of the noble metals by physical processes

Chris Ballhaus · Conny Bockrath · Cora Wohlgemuth-Ueberwasser · Vera Laurenz · Jasper Berndt

Received: 13 March 2006 / Accepted: 23 June 2006 / Published online: 15 September 2006

Abstract During partial melting in the earth's mantle, the noble metals become fractionated. Os, Ir, Ru, and Rh tend to remain in the mantle residue whereas Pt, Pd, and Re behave mildly incompatible and are sequestered to the silicate melt. There is consensus that sulfide plays a role in the fractionation process; the major noble metal repository in the mantle is sulfide, and most primitive mantle melts are sulfide-saturated when they leave their mantle sources. However, with sulfide–silicate partitioning, the fractionation cannot be modeled properly. All sulfide–silicate partition coefficients are so extremely high that a silicate melt segregating from a mantle source with residual sulfide should be largely platinum-group elements free. We offer a physical alternative to sulfide–silicate chemical partitioning and provide a mechanism of generating a noble metal-rich melt from a sulfide-saturated source: Because sulfide is at least partially molten at asthenospheric temperature, it will behave physically incompatible during melt segregation, and a silicate melt segregating from a mantle residue will entrain molten residual sulfide in suspension and incorporate it in the basaltic pool melt. The noble metal abundances of a basalt then become independent of sulfide–silicate chemical partitioning. They reflect the noble metal abundances in the drained sulfide fraction as well as the total amount of sulfide entrained. Contrary to convention, we suggest that a fertile, sulfide-rich mantle source has more potential to generate a noble metal-enriched basaltic melt than a refractory mantle source depleted by previous partial melting events.

Communicated by J. Hoefs.

C. Ballhaus (✉)
Mineralogisches Institut und Museum, Universität Bonn,
Poppelsdorfer Schloss, 53115 Bonn, Germany
e-mail: Ballhaus@uni-bonn.de

C. Ballhaus · C. Bockrath · C. Wohlgemuth-Ueberwasser · V. Laurenz · J. Berndt
Institut für Mineralogie, Universität Münster,
Corrensstr. 24, 48149 Münster, Germany

C. Bockrath
Landesmuseum Kärnten, Museumgasse 2,
9021 Klagenfurt, Austria

Introduction

When fertile upper mantle undergoes partial melting, the chemical elements are fractionated between the mantle residue and the partial silicate melt. The sense of fractionation is controlled by mineral/melt partition coefficients. The degree of fractionation is influenced by the degree of melting, the melting mode, and the modal abundances of mineral phases participating in the melting process. For most elements, especially for lithophile trace elements substituting for the major elements in silicates and oxides, there exists a well established order in terms of compatibility during mantle melting (cf. Hofmann 1997).

For the chalcophile elements, this is only partly true. Many of the elements with preference toward sulfide phases partition rather expectedly. Very often, they are surprisingly incompatible and fractionate into basaltic melts even though the mantle sources are thought to be sulfide-saturated. For example, Re, Pd, and sometimes Pt may be enriched in primitive mantle melts relative to the abundances in fertile mantle (Barnes et al. 1985,

1988, Fig. 1a), a fact that is hard to reconcile with sulfide-saturated residues. The experimentally determined sulfide–silicate coefficients reported for these elements, i.e., between 1,000 and 10^6 (Peach et al. 1990, 1994; Stone et al. 1990; Fleet et al. 1991, 1996, 1999; Bezmen et al. 1994; Crocket et al. 1997; Brenan and McDonough 2005), are so extremely high that a silicate melt in equilibrium with sulfide in the residue should be nearly noble metal free. The same objection is valid for the relative noble metal abundances. All primitive basalts regardless of melting degree and tectonic setting are depleted with respect to the refractory platinum-group elements (PGE) Os, Ir, and Ru, resulting in the characteristic positively sloping noble metal patterns. Again, none of the published experimental studies report differences in sulfide–silicate Ds that would match these patterns even broadly.

A possible solution to the problem is that sulfide does not generally survive partial silicate melting. Once sulfide is exhausted in the source, the PGE abundances are no longer limited by sulfide–silicate partition coefficients. Keays and coworkers (Hamlyn et al. 1985; Keays 1995) applied this concept to ore-forming processes, arguing that only melts from refractory mantle sources depleted in sulfide by previous melting events have the potential be sulfide undersaturated, and hence be rich enough in noble metals to form a PGE deposit. In turn, one would expect that basalts from fertile sources should be systematically poor in PGE because fertile sources are likely to rich in sulfide. However, this does not seem to be the case: basalts from the Loihi seamount (Hawaii) have Re and Pd concentrations 2.4 and 2.2 times the abundances of the primitive mantle (Bennett et al. 2000), yet they come from a source that experienced considerable enrichment by subducted crustal material (cf. Sobolev et al. 2000, 2005), likely to have been sulfide-rich.

Bockrath et al. (2004a) proposed a model to resolve these conflicts. Based on melting experiments with sulfide-saturated mantle material, they argued that molten sulfide in the mantle may be drained when silicate melt segregates from the matrix. They found that in partially molten upper mantle, sulfide is concentrated to a very large degree as immiscible droplets in silicate melt pockets. The implication of this observation is profound: if a basalt contains a drained sulfide component from the mantle, its PGE abundances become independent of chemical partitioning rules but reflect the amount of sulfide drained and the noble metals concentrated in that sulfide.

The sulfide entrainment model may explain the absolute noble metal abundances of a basalt, but it does not provide an answer as to how the noble metals are fractionated relative to each other. The fractionation should take place in the mantle, as mantle samples often have noble metal spectra broadly complementary to those of basalts (Fig. 1b). Obviously, a sulfide melt prior to entrainment in a silicate melt must coexist in the mantle source with another phase with equally high affinities toward the PGE, able to fractionate Os, Ir, and Ru even in competition with sulfide melt. Presumably, this phase is crystalline in order to be retained by the residue when silicate and sulfide melt segregate. The likely candidates are chromite (Capobianco and Drake 1990; Capobianco et al. 1994; Righter et al. 2004), discrete PGE phases (Borisov and Palme 2000; O'Hara et al. 2001), and crystalline monosulfide.

In this paper, we test experimentally whether this residual phase can be monosulfide. We report melting experiments to 3.5 GPa and 1,400°C with three sulfide compositions and explore the thermal stability of crystalline $(Fe, Ni, Cu)_{1-x}S$ monosulfide as a function of pressure, temperature, and sulfide composition. Monosulfide is a plausible residual phase for the

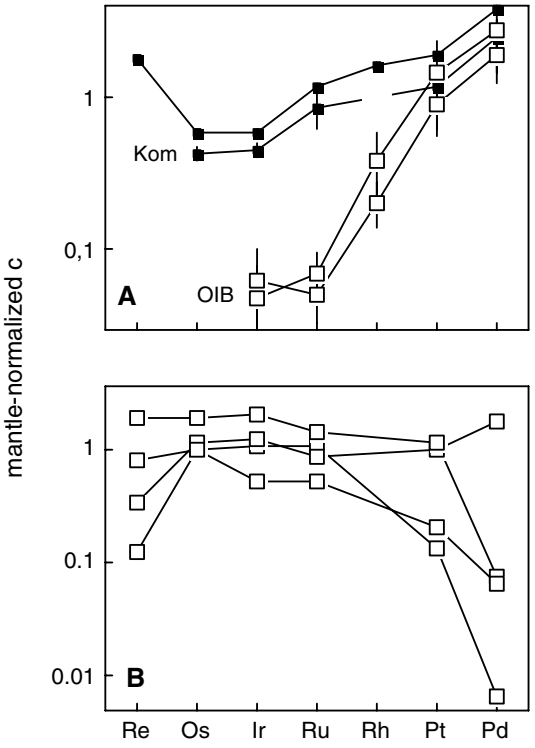

Fig. 1 Noble metal spectra of primitive mantle melts (**a**) and cratonic peridotite xenoliths (**b**). Data sources: Kostomuksha komatiites (Puchtel and Humayun 2002), Alexo komatiite (Meisel and Moser 2004), Greenland picrites (Philipp et al. 2001), Hawaiian picrites (Bennett et al. 2000), Lesotho xenoliths (Pearson et al. 2004)

following reasons: (1) Crystalline (Fe, Ni, Cu)$_{1-x}$S is known to incorporate Os, Ir, Ru, and Rh in preference to Pt and Pd (Ballhaus et al. 2001); hence, if a drained sulfide melt coexisted with monosulfide solid solution (mss) in the source, it will be depleted in Os, Ir, Ru, and Rh, imposing a positively sloping PGE pattern onto the basalt as commonly observed. (2) Many lithospheric mantle xenoliths carry two populations of sulfide, an FeS-rich monosulfide mostly included in silicates and a chemically variable generation of Cu–Ni-rich sulfides largely concentrated along grain boundaries (Lorand and Conquere 1983; Burton et al. 1999; Alard et al. 2000, 2005); potentially, these two types of sulfide witness ancient partial melting episodes in the two-phase (solid–liquid) field of mantle sulfide, frozen in when the samples cooled to lithopheric temperatures (Alard et al. 2002). And (3) endmember Fe$_{1-x}$S is thermally so stable that it can coexist with silicate melt at the pressure–temperature conditions of asthenospheric upper mantle (cf. Ryzhenko and Kennedy 1973).

Sulfide phase relations

Experiments with sulfide under upper mantle conditions are challenging. In the mantle, sulfide is a trace constituent not exceeding 600–700 ppm (Palme and O'Neill 2003). Therefore, sulfide compositions are entirely dominated by exchange equilibria with the major mantle phases, and hence react extremely sensitively to minor changes in pressure and temperature, as well as in the fugacities of S_2 and O_2 (f_{S_2} and f_{O_2}). In addition, unlike silicate melt, sulfide melt is not quenchable homogeneously, and therefore phase relations at magmatic temperature have to be inferred entirely from sulfide quench textures.

Starting compositions are listed in Table 1. Ni was set to 15.6 wt.% and approximated from the Fe–Ni exchange with mantle olivine, i.e., $NiO_{ol} + FeS_{sul} = FeO_{ol} + NiS_{sul}$. We have chosen an exchange coefficient ($K_D^{\text{sul–sil}}_{\text{Fe–Ni}}$) for this equilibrium of 15 and a relative f_{O_2} of FMQ (Doyle and Naldrett 1987; Brenan and Caciagli 2000) to simulate a moderately oxidized mantle (Ballhaus 1993). Cu shows a wide range, from 0.5 to 1.9 wt.%, appreciating that we do not know how much of the Cu in primitive mantle (~ 20 ppm; Palme and O'Neill 2003) actually resident in sulfide. Wet-chemical analyses of clinopyroxene separates from mantle rocks (Wedepohl 1974) suggest that clinopyroxene may contain Cu concentrations of up to several tens of ppm. This may mean that some proportion of the Cu in the upper mantle could be stored in silicate, although it is possible that some of the Cu assigned by Wedepohl (1974) to clinopyroxene may be due to sulfide inclusions (cf. Luguet et al. 2003). The least known variable is the S content. The metal/S ratio of mantle sulfide is a complex function of f_{S_2} and f_{O_2}, the Fe–Ni–Cu content of the sulfide, as well as pressure and temperature (cf. K_D equilibrium above). How these variables affect metal/S in detail is not known, and therefore to cover that uncertainty, we have chosen a range in atomic metal/S from 0.92 to 1.11, expecting that natural mantle sulfide will fall inside this range.

Table 1 Starting mixes used in this study (in wt.%)

Element	S1	S2	S3	S4
Fe	45.9	47.9	40.4	48.9
Ni	15.6	15.6	15.5	15.5
Cu	0.53	1.91	7.70	1.90
S	38.0	34.7	36.3	33.7
Atomic metal/S	0.93	1.06	0.98	1.11

All mixes contain ~20 ppm each of Re and PGE, added as chloride solutions. The metal/S atomic ratio is a measure of the oxidation state of the bulk sulfide

The starting sulfides were synthesized from metal powders and elemental S in evacuated SiO_2 glass tubes and reacted stepwise to sulfide at 200, 300, 500, and 700°C for ~ 40 h. To keep out oxygen, the tubes were repeatedly evacuated and flushed with Ar before sealing with an H_2–O_2 torch. We also added a trace of powdered boron nitride to scavenge any remaining O_2 and prevent magnetite as a phase and/or significant oxygen concentrations in sulfide melt. All experiments were carried out in SiO_2 glass: the 1-atm experiments in evacuated 6 mm outer-diameter tubes, and the higher-pressure piston cylinder experiments in 4 mm outer-diameter SiO_2 glass capsules welded shut on one side and sealed on the other side with a pyrex glass plug.

Typical quenching textures are summarized in Fig. 2. The 1 atm phase relations are easy to quench and interpret because quenching is done by dropping the tubes in cold water; hence is extremely rapid. In the piston cylinder press, however, inital quench rates are no better than 2 s for the first 200°, and this leaves ample time for back reaction between equilibrium phases, obscuring phase relations. To overcome this problem, we used for piston-cylinder experiments extra-long SiO_2 capsules that extend from the thermocouple to the bottom of the talc–pyrex assembly, encompassing a vertical temperature gradient of ~ 80°C. Long capsules have the advantage that a single experiment may show phase relations from subsolidus

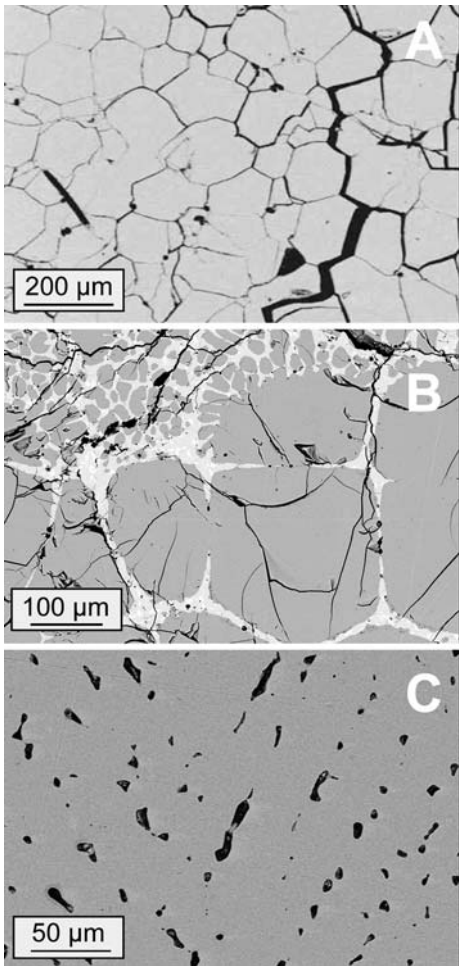

Fig. 2 Quench textures of sulfide experiments (BSE images). **a** Granular monosulfide crystals from a subsolidus run. **b** A "cumulate textured" experiment quenched in the two-phase (mss + liquid) field. The large rounded grains are equilibrium mss (*gray*) and the interstitial material is former sulfide melt, quenched heterogeneously to small rounded mss, light gray Cu-rich sulfides, and traces of a white Ni-dominated metallic phase. Note the effect of quench modification: larger sulfide melt pools precipitate mss in situ whereas sulfide melt wedged between equilibrium mss precipitate their mss component as overgrowth on equilibrium mss. **c** Homogeneous mss dendrites quenched from a superliquidus run; dendritic quench crystals outlined by bubbles of a vapor phase, exsolved from the sulfide melt during quenching, and concentrated by the rapidly growing mss dendrites at grain boundaries

to superliquidus temperature, greatly facilitating the interpretation of quench textures in terms of phase relations.

Runs at subsolidus temperature tend to return granular, highly friable sulfide grain aggregates, typically with 120° triple grain boundaries (Fig. 2a). The oxidized (low metal/S) composition S1 is single-phase mss at subsolidus temperature. S2 is also single-phase but only immediately below the solidus. At lower temperature, it recrystallizes to S-deficient mss and a Ni–Cu-enriched sulfide with higher metal/S, possibly intermediate solid solution (iss). The highly reduced composition S4 is at least three-phase at subsolidus temperature and crystallizes metal-deficient mss, an S-deficient Ni–Cu-sulfide (possibly iss), and tiny blebs of a Ni-rich metallic phase.

For all compositions in Table 1, the melting reaction is divariant in *P–T* space. When the two-phase (mss plus sulfide melt) field is reached, S1 and S2 develop "cumulus" textures (Fig. 2b) with rounded FeS-rich mss set in a matrix of Ni–Cu-rich interstitial sulfides quenched from sulfide melt. For the reduced S4 composition, the textural change upon melting is less obvious because S4 is also polyphase at subsolidus temperatures. The criterion to identify melting here was by back reaction: if at run conditions mss coexisted with a melt phase, it will react during quenching with the melt and develop Cu-enriched overgrowth rims and/or Cu-rich impregnations along contraction cracks (cf. Ballhaus et al. 2001).

As the liquidus temperature is approached, quench textures become more obscure. The liquidus curve may be positioned where charges quench single-phase mss (Fig. 2c), based on the assumption that a bulk composition that is single-phase at subsolidus temperature will also quench single-phase from a superheated melt. The liquidus curve was only determined for the most oxidized S1 sulfide, and no attempt was made to map the liquidi of the other compositions: We note that regardless of the bulk sulfide metal/S, equilibrium mss coexisting with sulfide melt was metal-deficient throughout (Fig. 3), even in runs with the most reduced composition S4, because variations in bulk Cu and/or bulk metal/S are accommodated almost entirely by the sulfide melt. Hence, in a fractional melting scenario where partial sulfide melt is constantly withdrawn from residual mss, final sulfide melting will not be determined by the liquidus temperature of the bulk sulfide composition but the melting point of the last monosulfide to disappear during fractional melting. The latter may be significantly more refractory than the bulk sulfide composition.

Solidus curves are summarized in Fig. 4. The compositional variable most influential on the temperature of first melting is the metal/S ratio. The S-rich composition S1 has a solidus curve in *P–T* space only slightly lower than the univariant melting curve of pure $Fe_{1-x}S$ (Ryzhenko and Kennedy 1973). The more reduced (metal-rich) compositions S2 and S4 experience first melting at considerably lower temperature. For S2, the solidus is displaced by about 250°C while maintaining the same positive slope as S1, and for the highly reduced S4 composition, we can only report a

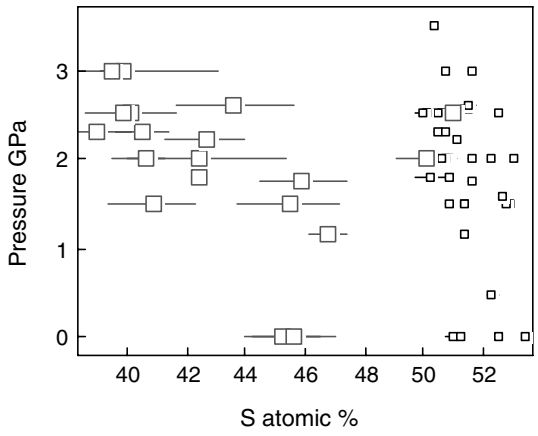

Fig. 3 Monosulfides (*small symbols*) coexisting with quenched sulfide melt (*open squares*) of all experiments in the two-phase field. Monosulfides vary little with respect to metal/S regardless of sulfide bulk composition. Fractionation with respect to the atomic metal/S ratio increases with increasing pressure. *Error bars* are one sigma of compositional heterogeneity

questionable solidus with no apparent pressure dependence. Note though that recognition of first melting in S4 is difficult as this composition is also polyphase at subsolidus temperature.

Platinum-group elements fractionation by residual monosulfide solid solution

It can also be tested chemically whether mss may be a stable phase in the asthenospheric upper mantle. We may calculate with mss-sulfide melt partition coefficients and realistic melting modes how the PGE should partition between mantle residue and silicate melt if the relative PGE abundances are buffered by residual mss. If the calculated spectra resemble PGE spectra of natural basalts, then there is a good chance that mss is a stable phase during mantle melting.

All starting mixes in Table 1 were doped with 20 ppm of each Re and PGE. The metals were added by microsyringe as acid chloride solutions. To prevent oxidation by the acid, notably of Fe metal, the solutions were added to the elemental S fractions of the mixes, then dried at 60°C for several hours, and only then were the base metals Fe, Ni, and Cu added and homogenized with S. Two of the partitioning experiments (OS-2 and OS-9) are with a new starting composition S3 that is equally oxidized as S1 (Table 1), but has more Cu_2S component, in order to widen the two-phase field and facilitate phase analysis by LA-ICP-MS. To one charge (OS-9), we also added 10 wt.% powdered hematite. Hematite is unstable with sulfide at run temperature and reacts with the $Fe_{1-x}S$ component to magnetite, driving f_{S_2} and f_{O_2} as well as the oxygen content in the sulfide melt to a maximum.

Coexisting mss and quenched sulfide melt were analyzed in six experimental charges with laser-ablation-ICP mass spectrometry. Ablation was done with a New Wave ArF excimer laser operating at 8 Hz and laser energies of ~ 5 J cm^{-2} into a He carrier gas. Beam diameters were 120 μm throughout to integrate as much as possible compositional heterogeneities in the quench phases. The ArF laser is coupled to a single-collector magnetic sector ICP Finnigan Element II mass spectrometer. Isotopes recorded are ^{34}S, ^{101}Ru, ^{103}Rh, ^{105}Pd, ^{185}Re, ^{189}Os, ^{191}Ir, and ^{195}Pt. Interferences are noted on ^{103}Rh and ^{105}Pd by $^{63}Cu^{40}Ar$ and $^{65}Cu^{40}Ar$; however, the contributions from these argides to Rh and Pd are negligibly small. We verified this by ablating pure Cu metal with the same conditions as the sulfide charges. Count rates of ^{105}Pd assignable to $^{65}Cu^{40}Ar$ were 725 cps or < 0.001% of the total Cu count rates. Count rates of ^{103}Rh from $^{63}Cu^{40}Ar$ were ~ 1,100 cps. Hence, for a sulfide with 2% Cu, the contributions from Cu argides to ^{105}Pd and ^{103}Rh are

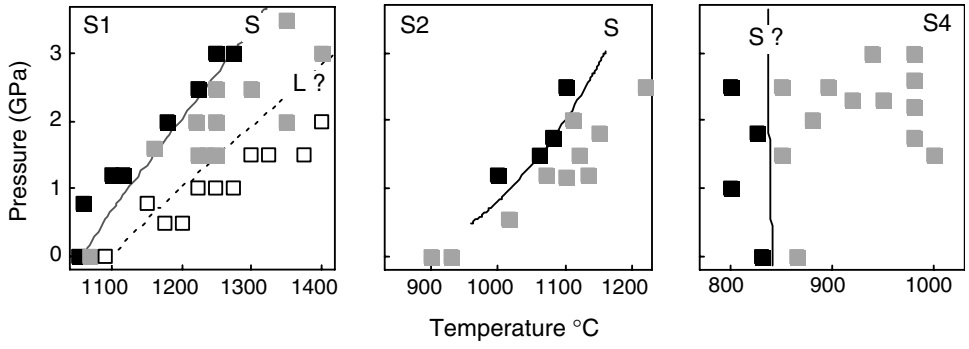

Fig. 4 Phase relations of sulfide starting compositions in *P–T* space. *Black symbols* are subsolidus runs, *gray squares* are charges with coexisting mss and sulfide melt (two-phase field), and *open squares* are superliquidus runs. *S* Solidus, *L* Liquidus. The major compositional control on the melting curve of mantle monosulfide is the atomic metal/S ratio

~ 15 and 20 cps, respectively, i.e., well within the gas background.

All count rates were normalized to ^{34}S and the average S content of the respective phase as analyzed by EPMA. No external standards were used; for the derivation of partition coefficients, there is no advantage in quantifying element concentrations as $D_{PGE}^{mss/sulfide\ melt}$ can be derived with the same precision by dividing the ^{34}S-corrected count rates of mss by the ^{34}S-corrected count rates recorded on quenched sulfide melt (cf. Ballhaus and Sylvester 2000).

Because sulfides are so reactive during quenching, it is important to demonstrate how well equilibrium compositions can be preserved. In Fig. 5, we show ^{34}S-normalized count rate ratios of the isotope ^{105}Pd of 15 consecutive ablations of quenched mss and sulfide melt pools from the 1-atm experiment OS-2. The two sigma relative standard deviations of the weighted arithmetic means are 9.5 and 6.3% on mss and sulfide melt, respectively, and quite typical for the other noble metals as well. In many experiments, mss is more heterogeneous than the quenched sulfide melt, perhaps

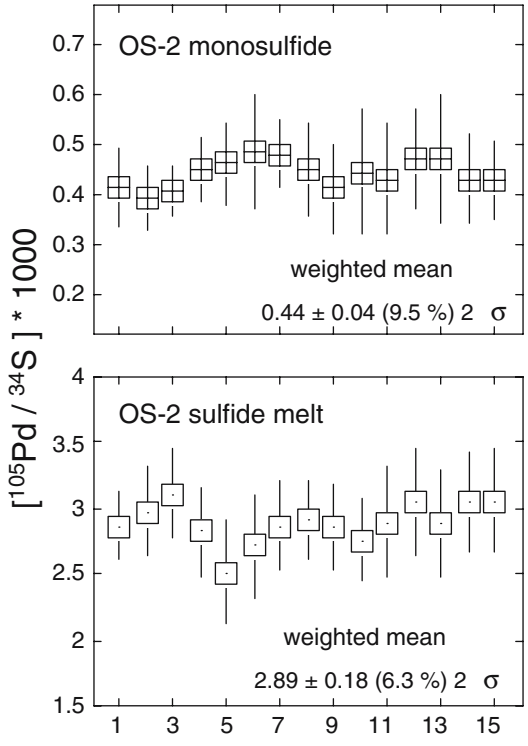

Fig. 5 Fifteen replicate analyses of mss and quenched sulfide melt of the 1 atm experiment OS-2, to assess compositional phase heterogeneity. ^{105}Pd normalized to ^{34}S counts and multiplied by 1,000. *Error bars* are two sigma and reflect the scatter in the ablation spectrum, most likely related to fluctuations in the plasma

illustrating the effect of back reaction during quenching which apparently imposes heterogeneity.

The mss-sulfide melt partition coefficients of six analyzed runs are displayed in Fig. 6 as a function of the melting point of the pure metals. They are broadly similar to previously published partition coefficients (Fleet et al. 1993; Li et al. 1996; Ballhaus et al. 2001; Brenan 2002). Re, Os, Ir, and Ru are moderately compatible with mss whereas Pt and Pd are highly incompatible. We noted an influence of oxidation state of the sulfide starting composition, expressed as bulk metal/S. The higher the bulk metal/S, the more efficiently the refractory elements Os, Ir, and Ru are fractionated from the less refractory Pt and Pd. In addition, under reduced (high metal/S) conditions, Ir appears to be slightly less compatible with mss than Os and Ru, confirming results by Mungall et al. (2005). The two high-pressure experiments analyzed for PGE suggest that pressure causes the Ds to converge relative to the 1 atm partition coefficients with the same starting composition. Whether this is real or a quenching artifact cannot be decided because higher-pressure runs suffer more back reaction than 1-atm runs. So what we note as a pressure effect on PGE partitioning might in reality be a metastable quenching effect (Table 2).

Discussion

Melting experiments with sulfide-bearing mantle material have shown (Bockrath et al. 2004a) that in partially molten mantle matrix, sulfide liquid resides as immiscible droplets in silicate melt. Given this distribution, it is likely that at least some part of the sulfide in basaltic melts originally was a drained component, inherited from the mantle source when the silicate melt segregated from the matrix. Such a model would render the noble metal concentrations in primitive basalts completely independent of sulfide–silicate partitioning, solving a long-standing problem in noble metal mantle geochemistry. With a drained sulfide component, we can explain why during mantle melting some chalcophile elements show incompatible behavior even though the mantle source is saturated with residual sulfide.

If sulfide draining is to dominate the PGE spectrum of a basaltic melt, the following conditions must be met: (1) At least some parts of the mantle region undergoing partial melting must remain sulfide-saturated until the silicate melt is segregated from the matrix; otherwise, no sulfide is left to be drained. (2) Since sulfide melt is denser than silicate melt, the

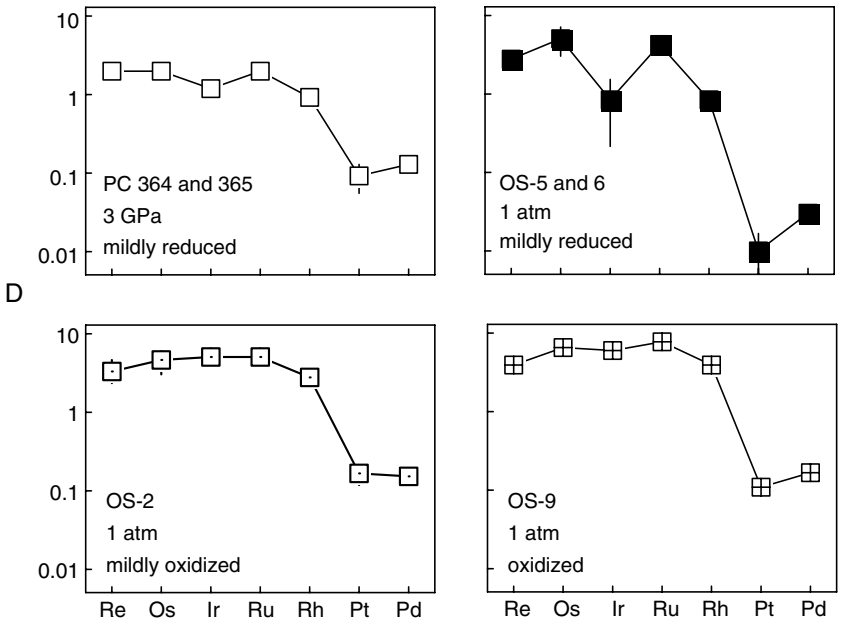

Fig. 6 Monosulfide–sulfide melt partition coefficients (D) of experimental charges (*error bars* = one sigma). For bulk and phase compositions consult Tables 1 and 2

ascent rate of a silicate melt that is segregated must exceed the settling speed of sulfide in suspension in silicate melt. (3) The melt conduits in a partially molten mantle must be wide enough to allow suspended sulfide melt droplets to be passed along with silicate melt. And (4) sulfide draining must reproduce the absolute noble metal abundances in basaltic melts.

Are silicate melts sulfide-saturated in the mantle source at the time of segregation?

Fertile mantle has 200–250 ppm S (Palme and O'Neill 2003) or 600–700 ppm FeS-dominated sulfide. The 1 atm S solubility in a typical basalt is ~ 1,000 ppm and somewhat higher in hot, MgO-rich mantle melts (Mathez 1976; O'Neill and Mavrogenes 2002). In a

Table 2 Phase compositions of experimental charges analyzed for Re and the PGE

Run no.	OS-9	PC-365	OS-6	PC-364	OS-5	OS-2
Starting mix	S3 + hem	S2	S2	S2	S2	S3
Temperature (°C)	980	1,150	900	1,175	930	1,020
Pressure (GPa)	0.001	3	0.001	3	0.001	0.001
Phases present	mss + mt + sl	mss + sl	mss + sl	mss + sl	mss + sl	mss + sl
Monosulfide solid solution (wt.% ± one sigma)						
Fe	45.5 ± 0.09	47.7 ± 0.10	50.9 ± 0.08	51.0 ± 0.29	51.6 ± 0.13	47.3 ± 0.28
Ni	13.3 ± 0.04	13.4 ± 0.19	10.3 ± 0.08	10.2 ± 0.08	9.7 ± 0.08	12.2 ± 0.19
Cu	1.97 ± 0.03	1.20 ± 0.00	0.99 ± 0.02	0.98 ± 0.03	0.90 ± 0.00	2.47 ± 0.34
S	38.7 ± 0.11	37.2 ± 0.17	36.7 ± 0.13	36.4 ± 0.17	36.7 ± 0.24	37.7 ± 0.36
Atomic metal/S	0.89 ± 0.01	0.95 ± 0.01	0.96 ± 0.01	0.97 ± 0.01	0.96 ± 0.01	0.93 ± 0.02
Sulfide melt (wt.% ± one sigma)						
Fe	40.8 ± 0.44	42.7 ± 3.63	33.3 ± 3.12	28.0 ± 2.94	37.7 ± 0.19	40.1 ± 1.20
Ni	15.5 ± 0.39	19.4 ± 4.26	29.8 ± 3.14	34.9 ± 2.97	24.6 ± 0.51	16.7 ± 2.16
Cu	8.17 ± 0.83	2.58 ± 0.94	3.93 ± 0.78	6.17 ± 2.48	3.70 ± 0.29	7.00 ± 3.78
S	35.1 ± 0.31	34.3 ± 1.89	31.5 ± 0.60	28.3 ± 1.46	31.9 ± 0.22	35.5 ± 0.71
Atomic metal/S	1.03 ± 0.03	1.06 ± 0.20	1.19 ± 0.15	1.35 ± 0.21	1.16 ± 0.02	1.00 ± 0.13
mss/melt partition coefficients						
D_{Re}	3.9 ± 0.3	1.8 ± 0.3	2.8 ± 0.2	2.2 ± 0.3	2.4 ± 0.2	3.4 ± 1.1
D_{Os}	6.7 ± 1.8	1.9 ± 0.4	5.2 ± 2.0	2.2 ± 0.2	3.7 ± 0.3	4.5 ± 1.5
D_{Ir}	6.3 ± 1.0	1.3 ± 0.4	0.9 ± 0.6	1.0 ± 0.2	1.3 ± 0.1	5.1 ± 1.2
D_{Ru}	7.5 ± 1.2	1.8 ± 0.3	4.2 ± 0.6	2.3 ± 0.3	4.1 ± 0.4	5.3 ± 1.2
D_{Rh}	4.0 ± 0.3	1.0 ± 0.1	0.9 ± 0.1	0.8 ± 0.1	0.8 ± 0.1	2.9 ± 0.4
D_{Pt}	0.11 ± 0.01	0.13 ± 0.06	0.01 ± 0.01	0.05 ± 0.01	0.01 ± 0.00	0.16 ± 0.04
D_{Pd}	0.16 ± 0.02	0.16 ± 0.02	0.03 ± 0.00	0.16 ± 0.02	0.03 ± 0.00	0.15 ± 0.03

mss monosulfide solid solution, *sl* quenched sulfide liquid, *mt* magnetite

simple batch melting scenario, sulfide would thus be eliminated in mantle regions where the partial melting degree exceeds 15–20% (cf. Rehkämper et al. 1999). Mantle melting, however, is fractional and basalts are pool melts (Kinzler and Grove 1992), i.e., a basalt receives contributions from melt fractions that originate by much smaller and much higher degrees of melting than the average degree of melting. At least the lower-degree melt contributions have a good chance to be sulfide saturated when they leave their source regions, and these melt fractions will impose a noble metal signature dominated by drained sulfide, whether or not in some parts of the melting volume sulfide was consumed. Moreover, S solubility falls with increasing pressure, by about a factor of 2 from 1 atm to 1 GPa (Mavrogenes and O'Neill 1999); so a basalt that is S undersaturated at the earth's surface may well be sulfide saturated at depth. Pressure effect plus fractional melting effect taken together render it likely that all basaltic pools melts receive fractions that were derived from S saturated mantle sources. These fractions will be PGE rich owing to sulfide entrained even if in some regions of the melting column sulfide did not survive.

Can dense sulfide melt be entrained in less dense silicate melt?

It must be possible to carry upward entrained dense sulfide melt against its tendency to settle in the less dense silicate melt. The average diameter of sulfide droplets in silicate mantle matrix measured by Bockrath and Ballhaus (2002) is around 1.5 μm (Fig. 7). These authors noted that sulfide droplets show little tendency to coalesce with time or to grow by diffusive sulfide transport (cf. de Bremon d'Ars et al. 2001), nor did they find that the average droplet sizes depended on the amount of sulfide added to an experimental charge. The settling speed of a 1.5 μm large sulfide droplet with a density of 4,000 kg m^{-3} is calculated with Stoke's law to ~ 15 cm $year^{-1}$ (viscosity from Kushiro et al. 1976). By comparison, magma ascent in partially molten mantle matrix is orders of magnitude faster (Elliott and Spiegelman 1993; Turner et al. 1996; Schubert et al. 2001), perhaps even as fast as meters per day (Rubin et al. 2005). Hence, from density considerations, there does not seem to be a problem that sulfide droplets, once entrained, can be drained by segregating silicate melt.

Are silicate melt conduits wide enough to let pass dispersed sulfide melt?

Mungall and Su (2005) rejected the sulfide draining model based on the claim that the melt conduits in partially molten mantle would not be wide enough to let pass disseminated sulfide melt droplets. Unfortunately, these authors did not constrain the widths of melt conduits nor did they discuss the principal melt segregation mode operating in the mantle; so, the validity of their argument is difficult to test. The least we can do is to broadly approximate the volumes of silicate melt pockets in a partially molten mantle matrix as a function of partial melting degree, and then compare these volumes with volumes of sulfide melt droplets as quantified by Bockrath and Ballhaus (2002).

Assume for simplicity that the silicate grains in crystalline mantle material are polyhedra whose centers are arranged in a cubic closed packing. The grain shapes at 0% melting are visualized as tetrahedra and octahedra in a ratio 2:1. This combination of shapes is chosen because it achieves complete tesselation of space. The grain sizes are defined as the distances between the centers of mineral grain polyhedra, and they are assumed here to be 500 μm, a reasonable grain size for upper mantle rocks. Let partial melting create melt pockets that are situated at the corners of crystal polyhedra. By analogy with the voids in a closed packing arrangement, we assume that the melt pockets have tetrahedral and octahedral shapes, and that there

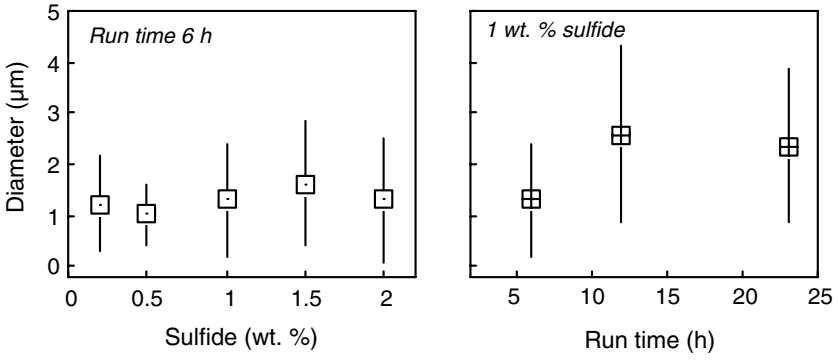

Fig. 7 Average diameters of sulfide melt droplets in silicate basaltic glass of partially molten peridotite measured with the image processing software Analysis on BSE images of polished experimental charges (see Bockrath et al. 2004a, b for details). All experiments at 1,360°C and 1 GPa in a piston-cylinder press, in a matrix of mantle silicates

are two tetrahedral and one octahedral melt pockets per mineral grain. For simplicity, we assume further that the edge lengths of the octahedral and octahedral melt pockets are identical.

This geometrical model, albeit simplistic, allows the volumes of melt pools at grain boundaries to be calculated as a function of grain size and degree of melting. Per three mineral grains (two tetrahedra and one octahedron) with a calculated total volume of ~ 0.088 mm^3, partial melting produces six tetrahedrally shaped and three octahedrally shaped melt pockets, all situated at grain corners. For a partial melting degree of ~ 0.15% and a uniform grain diameter of 500 μm, the tetrahedral and octahedral volumes are 4,910 and 19,642 μm^3, respectively. By comparison, sulfide melt droplets with averages of 1.5 μm across, as measured by Bockrath and Ballhaus (2002), only have volumes of ~ 3 μm^3.

In view of these volume relations, it would actually be surprising if sulfide droplets were not to be drained from the matrix once silicate melt interconnectivity is achieved. Moreover, with the segregation rates in MORB sources as deduced by Rubin et al. (2005), i.e., decades from the mantle source to the surface, the dominant segregation mode will not be by grain boundary percolation as implied by Mungall and Su (2005) but rather by channelized flow (cf. Turner et al. 1996; Korenaga and Kelemen 1998), even for extremely small melt proportions. Melt conduit widths then are no limiting factor anymore, and the objections by Mungall and Su (2005) toward sulfide entrainment become obsolete.

Are absolute and relative PGE abundances in basalt reproduced by sulfide draining?

For this calculation, we assume that prior to melt segregation, sulfide melt coexists with crystalline monosulfide. Because oxidized mss has the highest thermal stability, we calculate the PGE spectra with average partition coefficients of the most oxidized experiments OS-2 and OS-9, shown in Fig. 8. The PGE are distributed between the two sulfide phases according to the mss-sulfide melt partition coefficients. PGE fractionation at this stage is only at the grain scale between crystalline mss and droplets of sulfide melt.

Then silicate melt is segregated. Only the sulfide melt fraction is drained while mss as a crystalline phase remains in the matrix, along with all other crystalline phases. Let the fraction of molten sulfide to total sulfide be 0.5 (50% sulfide melting) and assume for simplicity that all molten sulfide is drained. Assume further that the silicate melting degree is 20% and that the melting model is batch melting. Then, compare the resulting model spectra (Fig. 8) with those of the respective natural equivalents (Fig. 1).

With respect to absolute PGE abundances, solely controlled by the PGE content in sulfide melt and the amount of sulfide entrained, we achieve an excellent match with natural abundances. Sulfide draining allows Pt–Pd concentrations in sulfide-saturated basaltic melts more than four times the mantle abundances. This is much better than with any other melting model where the PGE are controlled by sulfide–silicate partitioning (cf. Rehkämper et al. 1999; Mungall and Su 2005).

The relative noble metal abundances, here assumed to be controlled by residual mss, are reproduced less perfectly. For example, natural melts do not normally have positive Pt anomalies nor do mantle residues have negative Pt anomalies. The mantle-normalized Ir/Pd ratio of our model basalt, 0.16 ± 0.02, is at the upper end of natural melt ratios and in the komatiitic range (0.16–0.2; Brügmann et al. 1987; Puchtel and Humayun 2000; Meisel and Moser 2004). The enrichment in Os, Ir, and Ru in the model residue, around 1.1 times primitive mantle, is well matched by natural samples (Irvine et al. 2003; Pearson et al. 2004). Note though that Os–Ir–Ru enrichments in residual mantle are not

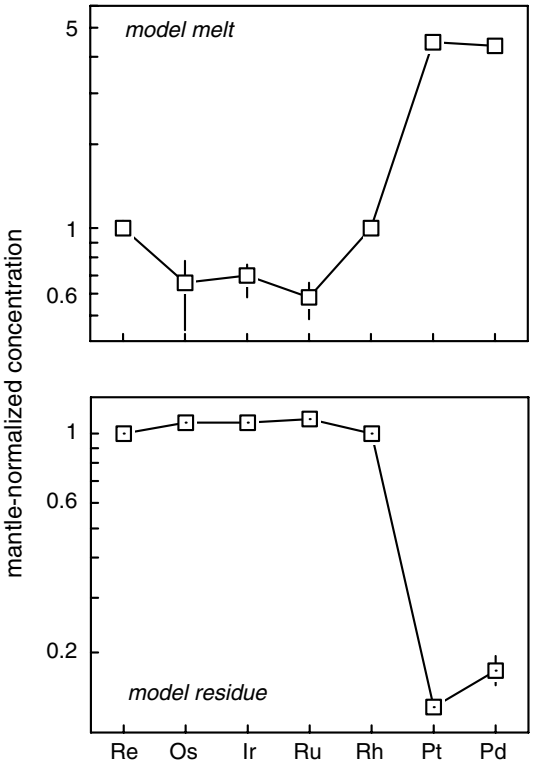

Fig. 8 Calculated noble metal patterns for a model melt and a model residue, using average mss-sulfide melt partition coefficients shown in Fig. 6c, d. For further assumptions see text

primarily controlled by partition coefficients during melting (so long as $D > 3$–4), but rather by the volume loss a mantle source experiences when silicate melt is segregated. Thus, if a natural residual mantle sample has Os–Ir–Ru concentrations greater than two times the primitive mantle values (cf. Büchl et al. 2002), one should be wary of an external component, e.g., discrete Os–Ir–Ru alloys (cf. Meibom et al. 2004) that were deposited from percolated silicate melts (see below).

The element most difficult to model with residual monsulfide is Re. Our calculation predicts that the model melt has a mantle-normalized Re concentration of 1.02. In nature, Re behaves more incompatibly. The most MgO-rich OIB typically have mantle-normalized Re abundances of 1.2–3 (cf. Reisberg et al. 1993; Widom and Shirey 1996; Hauri and Hart 1997; Lassiter and Hauri 1998; Bennett et al. 2000), and komatiites are similar ranging from ~1.7 to 3 (Brandon et al. 2003; Meisel and Moser 2004). Likewise, the modeled mantle-normalized Re/Os melt ratio (1.6 ± 0.3) is lower than that of primitive OIB and komatiite, which lie between 3 and 15. As for the Re abundances in residual mantle, our melting model is rather unspecific. If Re was affected only by melt extraction, with residual mss retaining Re in the source, Re should be as conservative as Os and Ir, and normalized Re/Os should be between 0.5 and 1. In natural residual mantle peridotite, Re and Re/Os can vary over two orders of magnitude (Büchl et al. 2002; Irvine et al. 2003; Pearson et al. 2004; Fig. 1b), probably because natural mantle samples not only record melt extraction events but also later metasomatic overprints that seem to mobilize Re and Pd in preference to the other PGE.

Sulfide draining recorded by Re-PGE abundances of natural mantle rocks?

Gao et al. (2002) recently documented a suite of lithospheric mantle xenoliths from Hannouba (China) whose compositions are entirely controlled by melt extraction. To our knowledge, this is the only suite of mantle rocks ever published in which the melt extraction signatures were not overprinted by later metasomatic events. We use this dataset to illustrate how in theory the noble metals should behave during melt extraction and sulfide draining.

The Hannouba xenolith suite ranges from fertile peridotite (Al_2O_3 = 3.5 wt.%) to refractory harzburgite (Al_2O_3 = 1.6 wt.%). Bulk S correlates with Al_2O_3 and falls with increasing degree of melt extraction. Note that this is a rare feature; normally in mantle rocks, S is highly mobile and easily disturbed by later metasomatic overprints (cf. Lorand et al. 2001, 2003, 2004; Alard et al. 2002; Irvine et al. 2003; Luguet et al. 2003). From the curvature in Fig. 9a, it would appear that S behaves slightly more compatibly than Al_2O_3, but in reality, the S depletion trend probably illustrates physical properties of sulfide melt, i.e., ease by which sulfide melt can be drained.

Out of the noble metals, only Re and Os were analyzed. Re correlates in a one-to-one fashion with S (Fig. 9b), and so do Re/Os and the $^{187}Os/^{188}Os$ isotopic ratios; the latter so tightly that Gao et al. (2002) could date the melt extraction event. Os, on the other hand, does not correlate with either bulk S or Al_2O_3 but behaves like a highly refractory element that is largely unaffected by melt extraction (Fig. 9c).

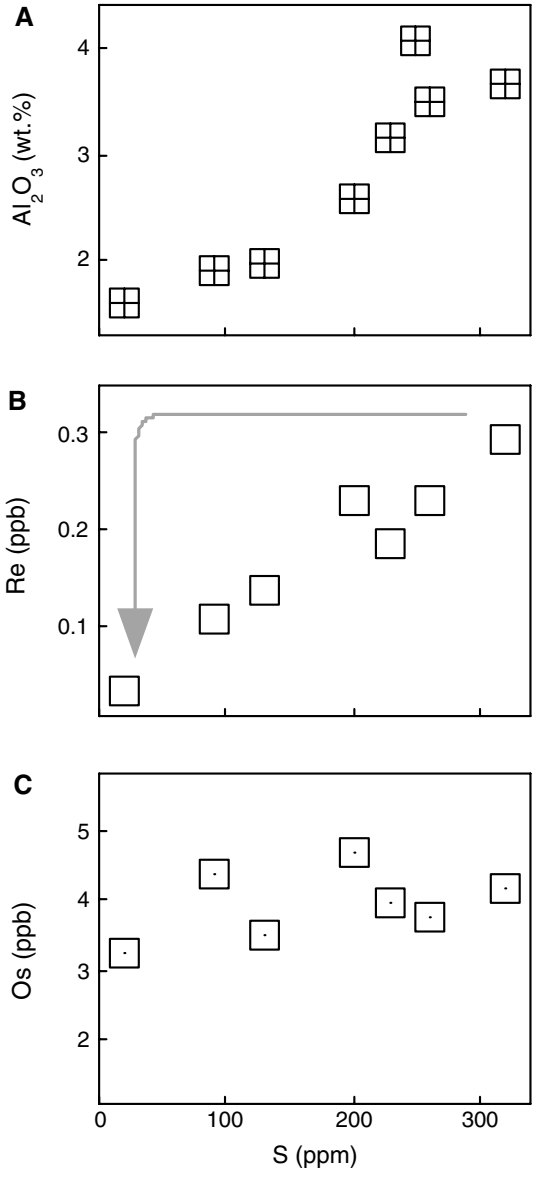

Fig. 9 Chemical signatures of peridotite xenoliths from Hannouba, China (Gao et al. 2002); see text for details

These correlations can only be explained sensibly if sulfide is drained as an immiscible liquid in suspension in silicate melt. The apparent compatibility of S, relative to that of Al_2O_3, reflects physical transport properties of sulfide melt, i.e., average droplet sizes, wetting properties against silicates, surface tension, average widths of segregation channels sulfide droplets have to pass through, etc. Re correlates with S because most of the Re is dissolved in the drained sulfide fraction, pretending a bulk chemical partition coefficient identical to that of S. No process other than sulfide draining can explain this Re–S one-to-one correlation. Conventional sulfide–silicate partitioning (cf. Mungall and Su 2005) would force Re to follow the arrow in Fig. 9b (cf. Lorand et al. 2004) because Re is highly chalcophile (Hauri and Hart 1997). Re would hang on as long as possible to a diminishing amount of sulfide and would only fall when the last fraction of sulfide becomes exhausted.

Os, on the other hand, must be concentrated in the Hannouba suites in a phase that is retained by the crystalline residue. For the Hannouba mantle suite, we can probably rule out that this phase was crystalline monosulfide because mss would also have concentrated Re (cf. partition coefficients in Fig. 6). Whether the residual phase is chrome spinel (Righter et al. 2004), a silicate phase (Burton et al. 2002; Brenan et al. 2005), or a PGE-rich alloy (cf. O'Hara et al. 2001; Meibom et al. 2004) is explored below.

Platinum-group elements fractionation during ascent and after emplacement

Platinum-group elements fractionation can also take place during ascent and after emplacement of the melt on the earth's surface. The key process is sulfide dissolution. Because sulfide solubility in basaltic melt increases with falling pressure (Mavrogenes and O'Neill 1999), sulfide droplets entrained from the mantle source may become dissolved as the basalt is decompressed on its passage to the surface. All the elements contained in sulfide, including the noble metals, are then released to the silicate melt. Further noble metal fractionation may now be by silicates or oxides, or if the silicate melt is PGE-saturated (cf. Borisov and Palme 1997, 2000), by discrete PGE phases.

Role of olivine and chromite?

In Fig. 10, we illustrate variations in PGE in a picrite–tholeiite suite from Greenland (Philipp et al. 2001) and a komatiite–tholeiite suite from Kostomuksha (Puchtel and Humayun 2000). In both suites, the major chemical control is by olivine fractionation, but only the picrites are co-saturated with chromite (Fig. 10a). Ir is depleted with falling Ni only in the chromite-saturated picrite–tholeiite suite (10C) whereas in the chromite-undersaturated komatiite–tholeiite suite, Ir (as well as Os and Ru) stays constant or even experiences slight enrichment as olivine fractionation proceeds. Pd exhibits incompatible behavior in both suites. Hence, the notion that olivine can fractionate some PGE in nature (Brügmann et al. 1987; Brenan et al. 2005) should be viewed with scepticism.

For chromite, the situation is different. We may calculate from the depletion trend in Fig. 10a, the $D_{\mathrm{Ir}}^{\text{chromite-melt}}$ by substituting the appropriate melt compositions in the batch fractionation equation $C_{\mathrm{L}} = C_0/[(D + F(1 - D)]$. Because the amount of chromite that can be precipitated from a silicate melt with 1,500–2,000 ppm Cr is so small, it is sufficient to assume batch fractionation. The most primitive Greenland picritic melt (C_0) has 2.2 ppb Ir and 1,440 ppm Cr. The most evolved tholeiitic melt (C_{L}) has 0.1 ppb Ir and 29 ppm Cr. The amount of chromite that may be fractionated from C_0 to C_{L} is ~ 0.3 wt.% if the chromite has 50 wt.% Cr_2O_3. F is the melt fraction left after removal of 0.3 wt.% chromite (= 0.997). The calculated $D_{\mathrm{Ir}}^{\mathrm{cr/L}}$ then is ~ 7,000.

But is a D of that magnitude realistic? At least it falls within the range of experimental $D_{\mathrm{Ir}}^{\text{chromite-melt}}$ reported by Righter et al. (2004) to range from 5 to 22,000. Note, however, that with a D = 7,000, early chromites on the liquidi of a picritic or komatiitic melts would contain ~ 700 ppm Ir, and this in addition to Os and Ru which behave similar to Ir (Philipp et al. 2001), i.e., should be similarly compatible with chromite. Surely, PGE concentrations of that magnitude would be detected during routine EMP analysis of high-temperature spinels, but that is not the case. In natural chromite cumulates enriched in the noble metals (Auge 1985; Garuti et al. 1999; Ahmed and Arai 2002; Matveev and Ballhaus 2002), the PGE, notably Os, Ir, and Ru, form discrete alloys and high-temperature sulfides attached to chromite (Bockrath et al. 2004b) but are never reported in solid solution in chromite. Some time ago, Hiemstra (1979), in an effort to explain Os–Ir–Ru enrichments in stratiform Bushveld chromitites, proposed a physical model by which some refractory PGE phases use the surfaces of chromite microliths as a nucleation substrate and are then fractionated as nuggets along with chromite (cf. Bockrath et al. 2004b). In variation diagrams (Fig. 10), such process could not be discriminated from chemical fractionation.

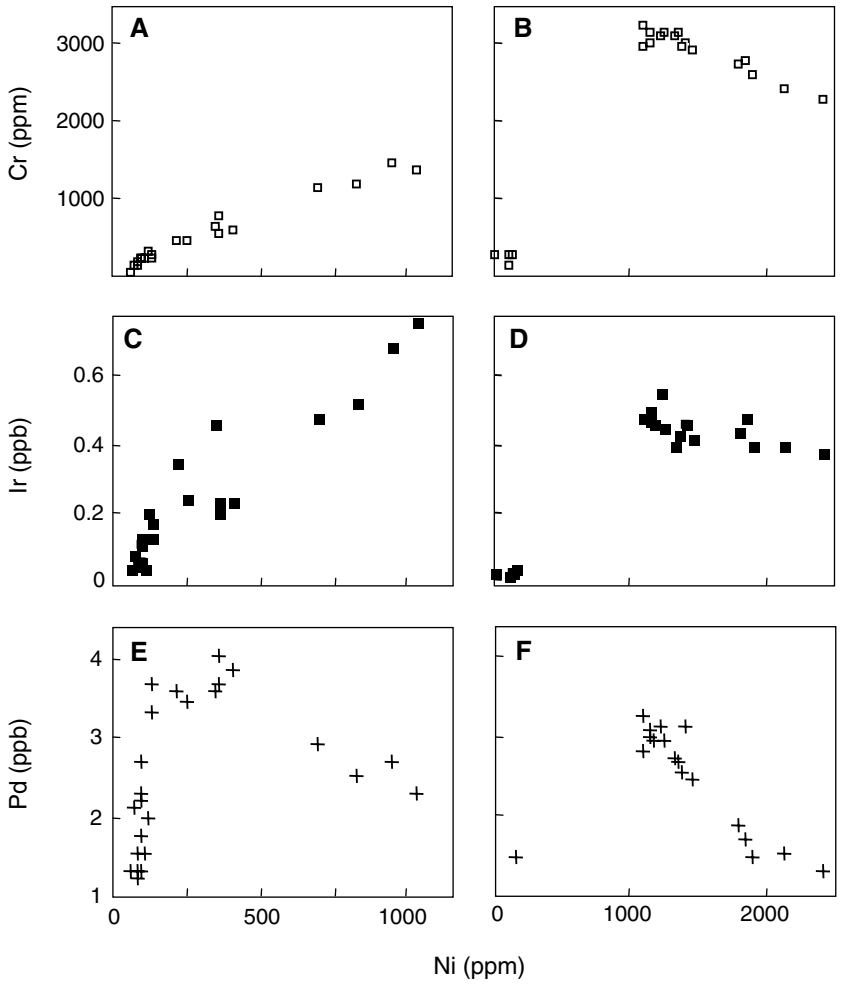

Fig. 10 Variations of Cr, Ir, and Pd in a picrite-tholeiite suite from Greenland (Philipp et al. 2001) and a komatiite–tholeiite suite from Kostomuksha (Puchtel and Humayun 2000). In both suites, the major chemical control is by olivine fractionation. Cr and Ni are in ppm, Ir and Pd are normalized to primitive mantle abundances (Palme and O'Neill 2003)

To follow up this possibility, we have carried out nucleation experiments to test how the PGE behave in sulfide-free PGE-oversaturated basaltic melts. A picrite (Rohrbach et al. 2005) was doped with 5 wt.% chromite component and 1 wt.% of a noble metal oxide (one experiment for each PGE). The metals were added to the picrite as oxides to ensure that any metallic nugget present in a quenched run product formed during the experiment. The experiments were performed at 0.5 GPa in a graphite capsule in a piston cylinder press, initially at 1,360°C for 5 h, then cooled with 10° h^{-1} to 1,200°C, kept there for another 5 h, and then quenched. Because PGE oxides are highly unstable at an oxygen fugacity imposed by the graphite capsule, the experiments simulate the fate of PGE released into a decompressing basaltic melt, after an entrained sulfide melt has been resorbed.

All charges crystallized olivine, euhedral chromite, and metallic noble metal alloys (Fig. 11). Ir and Ru form a near-infinite number of extremely small-sized metallic nuggets mostly attached to the edges and corners of chromite microliths (V. Laurenz 2005, unpublished thesis). Pt and Pd tend to crystallize to much fewer and much larger-sized metallic phases, most of which are suspended freely in silicate glass. Rh shows a behavior somewhere in between these extremes, with small alloys attached to chromite and larger metal grains suspended freely in glass. For Re and Os, we do not have data because both elements proved too volatile to be contained in the charge.

In Fig. 12, we quantify this size distribution and relate it to the melting points of the pure metals. The higher the melting point, the smaller the nuggets in the run products and the more pronounced their affinity to a chromite surface. When PGE are released to silicate melt following sulfide dissolution, the refractory PGE with affinity toward chromite surfaces may crystallize heterogeneously on chromite surfaces and may be fractionated ''piggyback'' along with chromite. PGE without that affinity may remain metastably in the silicate melt, with no chance to become depleted by fractionation of chromite. In our percentage concentration experiments, these elements precipitated as large-sized metallic lumps (Fig. 11c, d); however, at the

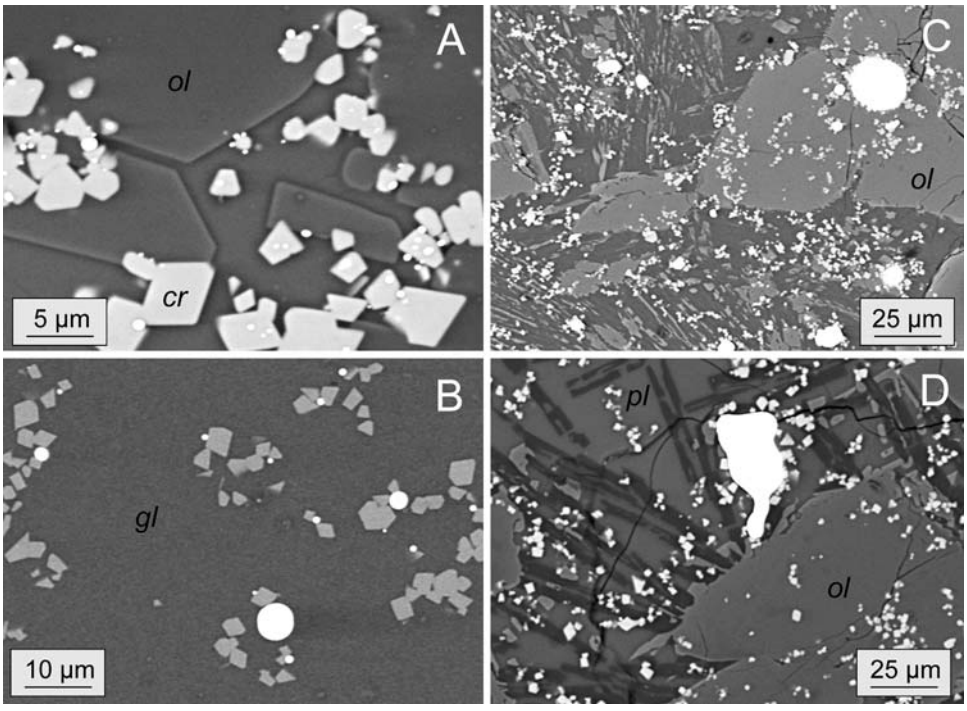

Fig. 11 BSE images of PGE nugget experiments. **a** Ir nuggets attached to chromite (*cr*). **b** Small Rh metal alloys attached to chromite, larger alloys suspended in glass (*gl*). **c** Large Pt metal alloys coexisting with chromite, olivine (*ol*), and quench plagioclase. **d** Large rounded Pd metal grain coexisting with olivine, skeletal quench plagioclase, and bright chromite microliths. All metal phases have variable Fe contents

much lower natural PGE concentrations, Pd and Pt would probably form metastable nano-sized metallic clusters (cf. Tredoux et al. 1995) that would remain suspended in silicate melt.

Figure 13 shows the effect of nugget fractionation on a PGE spectrum of a basaltic melt. Precipitation of chromite causes an anticlockwise rotation of the PGE pattern, by providing a nucleation substrate only to the most refractory PGE alloys. It is a plausible mechanism to explain why OIB have lower Os–Ir–Ru concentrations than komatiites, at near-identical Pt–Pd concentrations. Nugget formation is only possible at S-undersaturated conditions; note, if sulfide was present in addition to chromite, the PGE would simply dissolve in sulfide melt, and this would destabilize discrete alloys at the overall low PGE concentrations in basaltic melts (cf. Borisov and Palme 1997; Sattari et al. 2002). In addition, in the presence of sulfide, it would be impossible to fractionate the refractory PGE relative to Pd (cf. Fig. 10c, e). Nugget fractionation may work

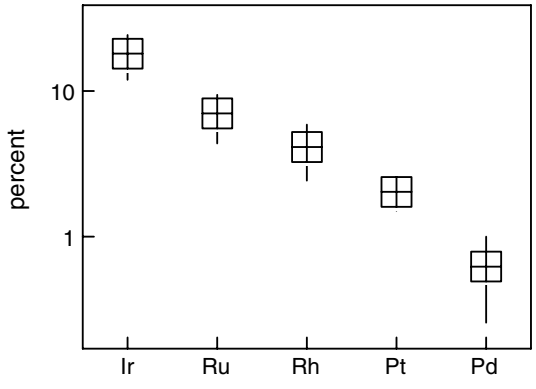

Fig. 12 Size distribution of noble metal alloys in the nugget experiments in Fig. 11. The sizes of noble metal alloys, between 800 and 1,700 grains per experiment, were measured with the image processing software analysis. The order on the *x*-axis is by the melting points of the pure metals. The *y*-axis is a measure for the size distribution of the metal nuggets. It quantifies the percentage of metal alloys necessary to accommodate 50% of the total alloy area measured in the BSE images. The higher that percentage, the smaller the individual metal alloys in the quenched run products, and the more distinct their tendency to nucleate on chromite surfaces

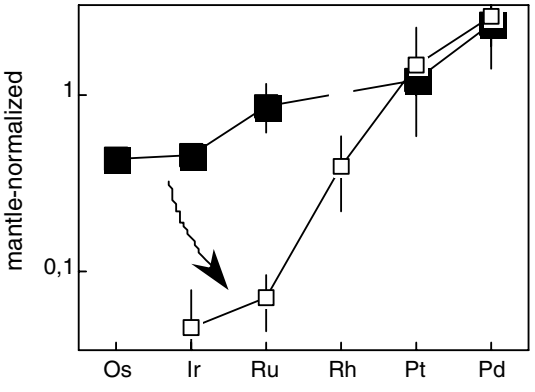

Fig. 13 Possible effect of Os–Ir–Ru alloy (''nugget'') fractionation on the PGE patterns of basaltic melts. Large dark squares are the averages of komatiites from Kostomuksha (Puchtel and Humayun 2000), and the small light squares are the averages of OIB analyzed by Greenough and Fryer (1990)

both within the mantle when chromite is precipitated by incongruent melting of Cr-diopside (Onuma and Tohara 1983) and during ascent of a chromite-saturated basaltic melt. Whenever mantle material has concentrations in the refractory PGE greater than two times the primitive mantle abundances, one should consider as reason nugget precipitation from a silicate melt that percolated through the mantle. Given enough time, nugget precipitation may also impose a grain-scale Os isotopic heterogeneity on the mantle, as observed by Meibom et al. (2004).

Under the extreme experimental conditions chosen by Capobianco and Drake (1990) and Capobianco et al. (1994), some PGE may indeed be forced inside oxide lattices. Note, however, that nugget fractionation via chomite has no limitations by partition coefficients and is equally effective under both oxidized and reduced conditions. Given the enormous range in Ir chromite-melt partition coefficients that Righter et al. (2004) report from just two chromite-melt experiments (i.e. 5 and 22,000), nugget fractionation simply is more likely than PGE substitution in the crystal lattice of chromite.

Role of late sulfide saturation

Sulfide solubility in silicate melt is sensitive to temperature and especially the polymerization degree of the melt. Therefore, cooling and olivine fractionation will drive basaltic melts sooner or later into S saturation. Many seemingly primitive basalts are sulfide-saturated, evident by tiny sulfide globules in silicate glass or in the mesostasis. When late sulfide saturation sets in, the PGE dissolved in the silicate melt at that stage are sequestered to sulfide melt. In the picrite–tholeiite suite in Fig. 11, sulfide saturation was reached at a Ni content of ~ 200–250 ppm, marked by the onset of Pd depletion.

Late sulfide saturation might be an important process to relate the PGE spectra of MORB to those of OIB. MORB are not systematically different to OIB with respect to relative PGE abundances; however, absolute PGE concentrations can be several orders lower (Fig. 14). This is the effect of late sulfide saturation: rapid depletion in absolute PGE concentrations without affecting the relative PGE abundances. Even though the sulfide–silicate partition coefficients are unlikely to be identical for all PGE, we cannot resolve differences by bulk chemical analysis because the partition coefficients are so extremely high. Hence, with respect to PGE and sulfide saturation, it appears that few MORB compositions could be termed primitive melts.

Conclusions

1. The noble metals in basaltic melts are fractionated more by physical processes than by chemical partitioning rules. Molten sulfide in asthenospheric upper mantle can be drained from the mantle matrix and entrained in a basaltic pool melt, when silicate melt is segregated. The noble metal concentrations in a basalt reflect the amount of sulfide drained and the noble metal abundances contained in that drained sulfide fraction. With sulfide draining, the noble metals in a basalt become largely independent of sulfide–silicate partition coefficients. With sulfide draining, it is possible to generate a basalt with bulk noble metals exceeding primitive mantle abundances even though the mantle source remains sulfide saturated. Chemically, the PGE may be highly compatible with sulfide; however, de facto they behave like incompatible elements because sulfide melt is a physically incompatible phase and easily entrained in a segregating silicate melt. Elements contained in a mobile sulfide fraction will tend to have bulk partition coefficients similar to that of S.

2. The process by which Os, Ir, and Ru are fractionated from Re, Pt, and Pd must take place largely inside the mantle. Fractionation happens in the presence of molten sulfide, since most basalts are S-saturated when they leave their source regions. Fractionation must involve a phase in addition to molten sulfide that is capable of concentrating Os, Ir, and Ru relative to Pt and Pd, even in competition with sulfide melt. A logical phase is crystalline monosulfide, as mss is known to incorporate Os, Ir, and Ru in preference to Pt and Pd. Thermally, an oxidized metal-deficient mss may indeed be stable enough to survive

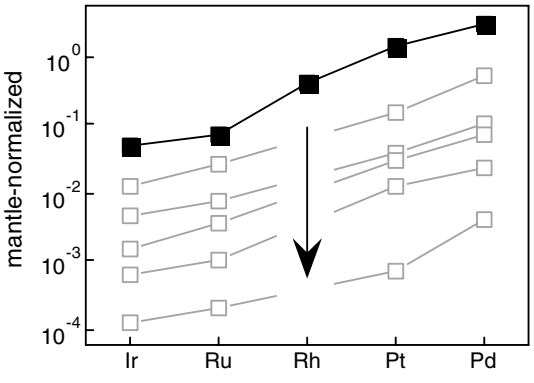

Fig. 14 Effect of low-pressure sulfide fractionation on the PGE spectra of basaltic melts. The spectrum with the dark symbols is the OIB average of Greenough and Fryer (1990), and the light spectra are individual MORB analyses from various localities analyzed by Rehkämper et al. (1999)

many partial silicate melting scenarios in the mantle; however, the relative noble metal abundances we calculate with residual mss deviate so strongly from abundances found in natural basalts, especially with respect to Re and Os, that we are inclined to discard mss as a residual phase during asthenospheric partial melting. Possible alternative phases are Os–Ir–Ru metallic alloys, common PGE phases in podiform and stratiform chromite ores as well as in residual mantle (Meibom et al. 2004), However, that would imply that in fertile sulfide-saturated mantle, not all PGE are hosted by sulfide (cf. Mitchell and Keays 1981).

3. Once sulfide is eliminated, either by excessive melting or by decompression of a basalt en route to the surface, the noble metals may also be fractionated by chromite. We doubt that in nature, PGE are incorporated to in the chromite lattice as extensively as suggested by Righter et al. (2004). Our preferred fractionation mode is again physical and involves ''nugget'' fractionation. In PGE-chromite-saturated but sulfide-undersaturated melts, the refractory PGE metals crystallize metallic alloys with a marked epitactic preference to chromite surfaces, whereas alloys of the less refractory PGE (Pt and Pd) seem to lack that chromite affinity and may remain suspended in silicate melt as nano-sized metallic cluster compounds (cf. Tredoux et al. 1995). Nugget fractionation causes an anticlockwise rotation of PGE spectra by depleting the refractory PGE more efficiently than Pt and Pd.

4. The last stages of PGE fractionation are sulfide-dominated and controlled by sulfide–silicate partitioning. Following emplacement on the earth's surface, most basaltic melts again reach sulfide saturation, triggered either by cooling and/or by olivine fractionation. Noble metals still in solution in silicate melt at this stage are rapidly sequested to the sulfide melt. There will be no relative PGE fractionation at this stage. The sulfide–silicate partition coefficients, although likely to be different, are so extremely high that an exsolving sulfide melt cannot discriminate among the PGE. Late sulfide fractionation is instrumental in generating an MORB spectrum. MORB have relative PGE abundances nearly identical to those of OIB, at absolute concentrations up to four orders of magnitude less than OIB, and many MORB are sulfide-saturated (Mathez 1976; Peach and Mathez 1990). This is exactly what one would expect with low-pressure, post-emplacement sulfide fractionation. Hence, with respect to sulfide, relatively few MORB are primitive melts (Bézos et al. 2005).

5. It is entrenched in the PGE literature that second-stage melts like boninites are unusually rich in Pd and Pt (Hamlyn et al. 1985; Hamyln and Keays 1986; Keays 1995). However, this notion does not stand up to closer examination. The idea dates from a time (i.e. the mid-1980s) when the database for Re and the PGE in basalts was much less than today and when it was taken for granted that the PGE abundances in a basalt could only be controlled by sulfide–silicate partitioning. Moreover, the comparison was made with MORB, as if MORB were typical first-stage melts derived from fertile mantle sources (cf. Hofmann 1997). We feel that the second-stage melting model is flawed. Boninites are not unusually rich in Pd and Pt (cf. Woodhead et al. 2002), and neither are MORB primitive with respect to PGE (Bézos et al. 2005, Fig. 14). The comparison should rather be made with S-undersaturated OIB, picrites, and perhaps komatiites. With these melts, boninites compare rather poorly. Average mantle-normalized Pd of boninites from the Izu-Bonin arc, analyzed by Woodhead et al. (2002) with isotope dilution, is ~ 0.9. In comparison, the Greenland picrites (Philipp et al. 2001) have mantle-normalized Pd of 1.9, the LEG 115 hot spot basalts reported by Greenough and Fryer (1990) are around 2.9, and Hawaiian picrites (Bennett et al. 2000) have mantle-normalized Pd around 0.98 (cf. Fig. 1). Hence, it appears that boninites are not unusually Pd-rich but rather depleted in Pd, as expected from melts that are generated in sources depleted by previous melt extraction events.

Acknowledgments Comments by J.-P. Lorand and an anonymous reviewer much improved the paper and are highly appreciated. Victor Vinograd helped with approximating the widths of melt conduits. The study was supported by the DFG grants BA 964/15, 964/23, and 964/24 to Chris Ballhaus.

References

Ahmed A, Arai S (2002) Unexpectedly high-PGE chromitite from the deeper mantle section of the northern Oman ophiolite and its tectonic implications. Contrib Mineral Petrol 143:263–278

Alard O, Griffin WL, Lorand JP, Jackson SE, O'Reilly SY (2000) Non-chondritic distribution of the highly siderophile elements in mantle sulphides. Nature 407:891–894

Alard O, Griffin WL, Pearson NJ, Lorand J-P, O'Reilly SY (2002) New insights into the Re-Os systematics of sub-continental lithospheric mantle from in-situ analysis of sulphides. Earth Planet Sci Lett 203:651–663

Alard O, Luguet A, Pearson NJ, Griffin WL, Lorand JP, Gannoun A, Burton KW, O'Reilly SY (2005) In situ Os isotopes in abyssal peridotites bridge the isotopic gap between MORBs and their source mantle. Nature 436:1005–1008

Auge T (1985) Platinum-group mineral inclusions in ophiolitic chromitite from the Vourinos complex, Greece. Can Mineral 23:163–171

Ballhaus C (1993) Oxidation states of lithospheric and asthenospheric upper mantle. Contrib Mineral Petrol 114:331–348

Ballhaus C, Sylvester P (2000) PGE enrichment processes in the Merensky reef. J Petrol 41:545–561

Ballhaus C, Tredoux M, Spaeth A (2001) Phase relations in the Fe-Ni-Cu-PGE-S system at magmatic temperature and application to massive sulfide ores of the Sudbury Igneous Complex. J Petrol 42:1911–1926

Barnes SJ, Boyd R, Korneliussen A, Nilsson LP, Often M, Pedersen RB, Robins B (1988) The use of mantle normalization and metal ratios in discriminating between the effects of partial melting, crystal fractionation and sulphide segregation on platinum-group elements, gold, nickel, and copper: examples from Norway. In: Prichard HM, Potts PJ, Bowles SJ, Cripp SJ (eds) Geoplatinum. Elsevier, London, pp 113–143

Barnes SJ, Naldrett AJ, Gorton MP (1985) The origin of the fractionation of platinum-group elements in terrestrial magmas. Chem Geol 53:303–323

Bennett VC, Norman MD, Garcia MO (2000), Rhenium and platinum group element abundances correlated with mantle source components in Hawaiian picrite: sulfides in the plume. Earth Planet Sci Lett 183:513–526

Bezmen NL, Asiv M, Brügmann GE, Romanenko IM, Naldrett AJ (1994) Distribution of Pd, Rh, Ru, Ir, Os, and Au between sulfide and silicate melts. Geochim Cosmochim Acta 58:1251–1260

Bézos A, Lorand JP, Hummler E, Gros M (2005) Platinum-group element systematics in mid-oceanic ridge basaltic glasses from the Pacific and Indian oceans. Geochim Cosmochim Acta 69:2613–2627

Bockrath C, Ballhaus C (2002) PGE fractionation between sulfide-bearing mantle and basaltic melt during partial melting and melt segregation. In: Proceedings of the 9th international platinum symposium, abstract with program, 21–25 July 2002, Billings, Montana, pp 41–43

Bockrath C, Ballhaus C, Holzheid A (2004a) Fractionation of the platinum-group elements during mantle melting. Science 305:1951–1953

Bockrath C, Ballhaus C, Holzheid A (2004b) Stabilities of laurite RuS_2 and monosulfide liquid solution at magmatic temperature. Chem Geol 208:265–271

Borisov A, Palme H (1997) Experimental determination of the solubility of platinum in silicate melts. Geochim Cosmochim Acta 61:4349–4357

Borisov A, Palme H (2000) Solubilities of noble metals in Fe-containing silicate melts as derived from experiments in Fe-free systems. Am Mineral 85:1665–1673

Brandon AD, Walker RJ, Puchtel IS, Becker H, Humayun M, Revillon S (2003) ^{186}Os-^{187}Os systematics of Gorgona Island komatiites: implications for early growth of the inner core. Earth Planet Sci Lett 206:411–426

de Bremon d'Ars JD, Arndt NT, Hallot E (2001) Analog experimental insights into the formation of magmatic sulfide deposits. Earth Planet Sci Lett 186:371–381

Brenan JM (2002) Re-Os fractionation in magmatic sulfide melt by monosulfide solid solution. Earth Planet Sci Lett 199:257–268

Brenan JM, Caciagli NC (2000) Fe-Ni exchange between olivine and sulphide liquid: Implications for oxygen barometry in sulphide-saturated magmas. Geochim Cosmochim Acta 64:307–320

Brenan JM, McDonough WF (2005) Fractionation of highly siderophile elements (HSEs) by sulfide-silicate partitioning: a new spin. In: Abstracts of the AGU Fall Meeting V41D-1502

Brenan JM, McDonough WF, Ash R (2005) An experimental study of the solubility and partitioning of iridium, osmium and gold between olivine and silicate melt. Earth Planet Sci Lett 237:855–872

Brügmann GE, Arndt NT, Hofmann AW, Tobschall HJ (1987) Noble metal abundances in komatiite suites from Alexo, Ontario, and Gorgona-Island Colombia. Geochim Cosmochim Acta 51:2159–2169

Büchl A, Brügmann G, Batanova VG, Münker C, Hofmann AW (2002) Melt percolation monitored by Os isotopes and HSE abundances: a case study from the mantle section of the Troodos ophiolite, Cyprus. Earth Planet Sci Lett 204:385–402

Burton KW, Schiano P, Birck J-L, Allegre CJ (1999) Osmium isotope disequilibrium between mantle minerals in a spinel-lherzolite. Earth Planet Sci Lett 172:311–322

Burton KW, Gannoun A, Birck J-L, Allegre CJ, Schiano P, Clocchiatti R, Alard O (2002) The compatibility of rhenium and osmium in natural olivine and their behaviour during mantle melting and basalt genesis. Earth Planet Sci Lett 198:63–76

Capobianco CJ, Drake MJ (1990) Partitioning of ruthenium, rhodium, and palladium between spinel and silicate melt and implications for platinum group element fractionation trends. Geochim Cosmochim Acta 54:869–874

Capobianco CJ, Hervig RL, Drake MJ (1994) Experiments on crystal liquid partitioning of Ru, Rh and Pd for magnetite and hematite solid-solutions crystallized from silicate melt. Chem Geol 113:23–43

Crocket JH, Fleet ME, Stone WE (1997) Implications of composition for experimental partitioning of platinum-group elements and gold between sulfide liquid and basalt melt: the significance of nickel content. Geochim Cosmochim Acta 61:4139–4149

Doyle C, Naldrett AJ (1987) The oxygen content of sulfide magma and its effect on the partitioning of nickel between coexisting olivine and molten ores. Econ Geol 82:208–211

Elliot T, Spiegelman M (1993) Consequence of melt transport for uranium series disequilibrium in young lavas. Earth Planet Sci Lett 118:1–20

Fleet ME, Crocket JH, Stone WE (1996) Partitioning of platinum-group elements (Os, Ir, Ru, Pt, Pd) and gold between sulfide liquid and basalt melt Geochim Cosmochim Acta 60:2397–2412

Fleet ME, Stone WE, Crocket JH (1991) Partitioning of palladium, iridium, and platinum between sulfide liquid and basalt melt; effects of melt composition, concentration, and oxygen fugacity. Geochim Cosmochim Acta 55:2545–2554

Fleet ME, Chryssoulis SL, Szone WE, Weisener CG (1993) Partitioning of platinum-group elements and Au in the Fe-Ni-Cu-S system—experiments on the fractional crystallization of sulfide melt. Contrib Mineral Petr 115:36–44

Fleet ME, Crocket JH, Menghua Li, Stone WE (1999) Laboratory partitioning of platinum-group elements (PGE) and gold with application to magmatic sulfide-PGE deposits. Lithos 47:127–144

Gao S, Rudnick RL, Carlson RW, McDonough WF, Liu L-S (2002) Re-Os evidence for replacement of ancient mantle lithosphere beneath the North China craton. Earth Planet Sci Lett 198:307–322

Garuti G, Zaccarini F, Moloshag V, Alimov V (1999) Platinum-group minerals as indicators of sulfur fugacity in ophiolitic upper mantle: an example from chromitites of the Ray-Iz ultramafic complex, Polar Urals, Russia. Can Mineral 37:1099–1115

Greenough JD, Fryer BJ (1990) Distribution of gold, palladium, rhodium, ruthenium, and iridium in LEG 115 hotspot basalts: Implications for magmatic processes. Proc ODP 115:71–84

Hamlyn PR, Keays RR (1986) Sulfur saturation and 2nd-stage melts—application to the Bushveld platinum metal deposits. Econ Geol 81:1431–1445

Hamlyn PR, Keays RR, Cameron WE, Crawford AJ, Waldron HM (1985) Precious metals in magnesian low-Ti lavas: implication for metallogenesis and sulfur saturation in primitive magmas. Geochim Cosmochim Acta 49:1797–1811

Hauri EH, Hart SR (1997) Rhenium abundances and systematics in oceanic basalts. Chem Geol 139:185–205

Hiemstra SA (1979) The role of collectors in the formation of the platinum deposits in the Bushveld complex. Can Miner 17:469–482

Hofmann AW (1997) Mantle geochemistry: the message from oceanic volcanism. Nature 385:221–229

Irvine GJ, Pearson DG, Kjarsgaard BA, Carlson RW, Kopylova MG, Dreibus G (2003) A Re-Os isotope and PGE study of kimberlite-derived peridotite xenoliths from Somerset Island and a comparison to the Slave and Kaapvaal cratons. Lithos 71:461–488

Keays RR (1995) The role of komatiitic and picritic magmatism and S-saturation in the formation of ore deposits. Lithos 34:1–18

Kinzler RJ, Grove TL (1992) Primary magmas of midocean ridge basalts 2. Applications. J Geophys Res 97:6907–6926

Korenaga J, Kelemen PB (1998) Melt migration through the oceanic lower crust: a constraint from melt percolation modeling with finite solid diffusion. Earth Planet Sci Lett 156:1–11

Kushiro I, Yoder HS, Mysen BO (1976) Viscosities of basalt and andesite melts at high pressures. J Geophys Res 81:6351–6356

Lassiter JC, Hauri EH (1998) Osmium-isotope variations in Hawaiian lavas: evidence for recycled oceanic lithosphere in the Hawaiian plume. Earth Planet Sci Lett 164:483–496

Li C, Barnes SJ, Makovicky E, Rose-Hansen J, Makovicky M (1996) Partitioning of nickel, copper, iridium, rhodium, platinum and palladium between monosulfide solid solution and sulfide liquid: effects of composition and temperature. Geochim Cosmochim Acta 60:1231–1238

Lorand JP, Alard O (2001) Platinum-group element abundances in the upper mantle: new constraints from in-situ and whole-rock analyses of Massif Central xenoliths (France). Geochim Cosmochim Acta 65:2789–2806

Lorand JP, Conquéré F (1983) Contribution à l'étude des sulfures dans les enclaves de lherzolites à spinell des basaltes alcalins (Massif Central et du Languedoc, France). Bull Minéral 106:585–606

Lorand J-P, Reisberg L, Bedini LM (2003) Platinum-group elements and melt percolation processes in Sidamo spinel peridotite xenoliths, Ethiopia, East African Rift. Chem Geol 196:57–75

Lorand J-P, Delpech G, Gréoire M, Moine B, O'Reilly SY, Cottin J-Y (2004) Platinum-group elements and the multistage metasomatic history of Kerguelen lithospheric mantle (South Indian Ocean). Chem Geol 208:195–215

Luguet A, Lorand J-P, Seyler M (2003) Sulfide petrology and highly siderophile element geochemistry of absyssal peridotites: a coupled study of samples from the Kane fracture zone (45°W 23°20N, MARK Area, Atlantic Ocean). Geochim Cosmochim Acta 67:1553–1570

Mathez EA (1976) Sulfur solubility and magmatic sulfides in submarine basalt glass. J Geophys Res 81:4269–4276

Matveev S, Ballhaus C (2002) Role of water in the origin of podiform chromitite deposits. Earth Planet Sci Lett 203:235–243

Mavrogenes J, O'Neill HStC (1999) The relative effects of pressure, temperature and oxygen fugacity on the solubility of sulfide in mafic magmas. Geochim Cosmochim Acta 63:1173–1180

Meibom A, Frei R, Sleep NH (2004) Osmium isotopic compositions of Os-rich platinum group element alloys from the Klamath and Siskiyou mountains. J Geophys Res 109:B02203

Meisel T, Moser J (2004) Reference materials for geochemical PGE analysis: new analytical data for Ru, Rh, Pd, Os, Ir, Pt and Re by isotope dilution ICP-MS in 11 geological reference materials. Chem Geol 208:319–338

Mitchell RH, Keays RR (1981) Abundance and distribution of gold, palladium and iridium in some spinel and garnet lherzolites—implications for the nature and origin of precious metal-rich intergranular components in the upper mantle. Geochim Cosmochim Acta 45:2425–2442

Mungall JE, Su S (2005) Interfacial tension between magmatic sulfide and silicate liquidus: constraints on kinetics of sulfide liquation and sulfide migration through silicate rocks. Earth Planet Sci Lett 234:135–149

Mungall JE, Andrews DRA, Cabri LJ, Sylvester PJ, Tubrett M (2005) Partitioning of Cu, Ni, Au, and platinum-group elements between monosulfide solid solution and sulfide melt under controlled oxygen and sulfur fugacities. Geochim Cosmochim Acta 69:4349–4360

O'Hara MJ, Fry N, Prichard HM (2001) Minor phases as carriers of trace elements in non-modal crystal-liquid separation processes II: illustrations and bearing on behaviour of REE, U, Th and the PGE in igneous processes. J Petrol 42:1887–1910

O'Neill HStC, Mavrogenes JA (2002) The sulfide capacity and the sulfur content at sulfide saturation of silicate melts at 1400 degrees C and 1 bar. J Petrol 43:1049–1087

Onuma K, Tohara T (1983) Effect of chromium on phase relations in the join forsterite-anorthite-diopside in air at 1-atm. Contrib Mineral Petrol 84:174–181

Palme H, O'Neill HStC (2003) In: Carlson RW (ed) Treatise of geochemistry, vol 2. The Mantle and Core, Elsevier Amsterdam, pp1–38

Peach CL, Mathez EA (1990) Sulfide melt silicate melt distribution coefficients for nickel and iron and implications for the distribution of other chalcophile elements. Geochim Cosmochim Acta 57:3013–3021

Peach CL, Mathez EA, Keays RR (1990) Sulfide melt—silicate melt distribution coefficients for noble metals and other chalcophile elements as deduced from MORB: implications for partial melting. Geochim Cosmochim Acta 54:3379–3389

Peach CL, Mathez EA, Keays RR, Reeves SJ (1994) Experimentally determined sulfide melt-silicate melt partition coefficients for iridium and palladium. Chem Geol 117:361–377

Pearson DG, Irvine GJ, Ionov DA, Boyd FR, Dreibus GE (2004) Re-Os isotope systematics and platinum group element fractionation during mantle melt extraction: a study of massif and xenolith peridotite suites. Chem Geol 208:29–59

Philipp H, Eckhardt JD, Puchelt H (2001) Platinum-group elements (PGE) in basalts of the seaward dipping reflector sequence, SE Greenland coast. J Petrol 42:407–432

Puchtel I, Humayun M (2000) Platinum group elements in Kostomuksha komatiites and basalts: implications for oceanic crust recycling and core-mantle interaction. Geochim Cosmochim Acta 64:4227–4242

Rehkämper M, Halliday AN, Fitton JG, Lee D-C, Wieneke M, Arndt NT (1999) Ir, Ru, Pt, and Pd in basalts and komatiites: New constraints for the geochemical behavior of the platinum-group elements in the mantle. Geochim Cosmochim Acta 63:3915–3934

Reisberg L, Zindler A, Marcantonio F, White W, Wyman D, Weaver B (1993) Os isotope systematics in ocean island basalts. Earth Planet Sci Lett 120:149–167

Righter K, Campbell AJ, Humayun M, Hervig RL (2004) Partitioning of Ru, Rh, Pd, Re, Ir, and Au between Cr-bearing spinel, olivine, pyroxene and silicate melt. Geochim Cosmochim Acta 68:867–880

Rohrbach A, Schuth S, Ballhaus C, Münker C, Matveev S, Qopoto C (2005) Petrological constraints on the origin of arc picrites, New Georgia Group, Solomon Islands. Contrib Mineral Petrol 149:685–698

Rubin KH, van der Zander I, Smith MC, Bergmanis EC (2005) Minimum speed limit for ocean ridge magmatism from Pb-210-Ra-226-Th-230 disequilibria. Nature 437:534–538

Ryzhenko B, Kennedy GC (1973) Effect of pressure on eutectic in system Fe-FeS. Am J Sci 273:803–810

Sattari P, Brenan JM, Horn I, McDonough WF (2002) Experimental constraints on the sulfide-silicate and chromite-silicate melt partitioning behavior of rhenium and platinum-group elements. Econ Geol 97:385–398

Schubert G, Turcotte DL, Olson P (2001) Mantle convection in the earth and planets. Cambridge University Press, Cambridge, 940p

Sobolev AV, Hofmann AW, Nikogosian IK (2000) Recycled oceanic crust observed in ghost plagioclase within the source of Mauna Loa lavas. Nature 404:986–990

Sobolev AV, Hofmann AW, Sobolev SV, Nikogosian IK (2005) An olivine-free mantle source of Hawaiian shield basalts. Nature 434:590–597

Stone WE, Crocket JH, Fleet ME (1990) Partitioning of palladium, iridium, platinum, and gold between sulfide liquid and basalt melt at 1200 degrees C. Geochim Cosmochim Acta 54:2341–2344

Tredoux M, Lindsey NM, Davies G, McDonald I (1995) The fractionation of platinum group elements in magmatic systems, with the suggestion of a novel causal mechanism. South Afr J Geol 98:157–167

Turner S, Hawkesworth C, van Calsteren P, Heath E, Macdonald R, Black S (1996) U-series isotopes and descructive plate margin magma genesis in the Lesser Antilles. Earth Planet Sci Lett 142:191–207

Wedepohl KH (1974) Copper. In: Wedepohl KH (ed) Handbook of geochemistry, vol 2, part 3. Springer, Berlin Heidelburg New York

Widom E, Shirey SB (1996) Os isotopic systematics in the azozes: implications for mantle plume sources. Earth Planet Sci Lett 142:451–465

Woodhead SJ, Pearson DG, Thirlwall MF (2002) A platinum group element and Re–Os isotope investigation of siderophile element recycling in subduction zones: comparison of Grenada, Lesser Antilles arc, and the Izo-Bonin arc. J Petrol 43:171–198